

Cite this: *Chem. Sci.*, 2023, 14, 5712

All publication charges for this article have been paid for by the Royal Society of Chemistry

Received 29th March 2023
Accepted 29th April 2023

DOI: 10.1039/d3sc01637d

rsc.li/chemical-science

Computational molecular refinement to enhance enantioselectivity by reinforcing hydrogen bonding interactions in major reaction pathway†

Taishi Nakanishi and Masahiro Terada *

Computational analyses have revealed that the distortion of a catalyst and the substrates and their interactions are key to determining the stability of the transition state. Hence, two strategies “distortion strategy” and “interaction strategy” can be proposed for improving enantiomeric excess in enantioselective reactions. The “distortion strategy” is used as a conventional approach that destabilizes the TS (transition state) of the minor pathway. On the other hand, the “interaction strategy” focuses on the stabilization of the TS of the major pathway in which an enhancement of the reaction rate is expected. To realize this strategy, we envisioned the TS stabilization of the major reaction pathway by reinforcing hydrogen bonding and adopted the chiral phosphoric acid-catalysed enantioselective Diels–Alder reaction of 2-vinylquinolines with dienylcarbamates. The intended “interaction strategy” led to remarkable improvements in the enantioselectivity and reaction rate.

Introduction

The development of enantioselective catalysis using a chiral catalyst has evolved into an active area of research over the past half-century. In current organic synthesis, catalytic enantioselective reactions are considered one of the indispensable methodologies for affording enantioenriched compounds in an efficient fashion. However, the development of catalytic enantioselective reactions requires enormous effort and costs to optimize not only the catalyst structure but also other reaction conditions. Moreover, in some cases, even substrate modifications are necessary to achieve high performance in terms of catalytic efficiency and stereochemical control. As a way to overcome these inherent difficulties, computational studies have been widely applied to the design of catalyst molecules and reaction systems to achieve highly efficient enantioselective catalysis in recent years.¹ Indeed, clarifying the structural features of transition states (TSs) that afford enantiomeric products by means of DFT calculations are helpful to improve the stereochemical outcome through rational refinement of the catalyst molecule and the reaction system.²

Among computational approaches reported thus far, the distortion/interaction analysis has been recognized as an intriguing method to characterize TSs.³ On the basis of this analytical method, two strategies can be proposed, which are aimed at improving enantioselectivity. One approach is the

“distortion strategy” (Fig. 1, strategy A), and the other is the “interaction strategy” (Fig. 1, strategy B). The former strategy is commonly used as a conventional approach mainly to destabilize **minor-TS** (the transition state of the minor reaction pathway) by the repulsive steric effect. This strategy offers the advantage of simplicity of designing catalyst molecules and reaction systems, because the steric effect is readily predictable from the TS structures. In addition, a relatively large difference in free energy is anticipated between **major-TS** (the transition state of the major reaction pathway) and **minor-TS**.^{2c,d,f,g} However, in some cases, the approach results in unpredictable

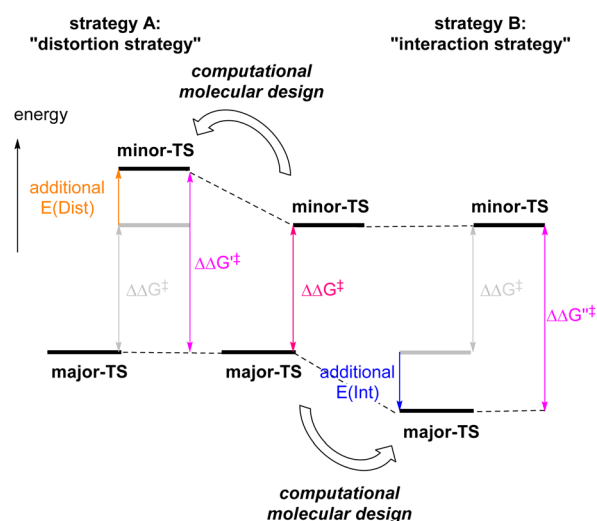


Fig. 1 Strategies for computational molecular design.

Department of Chemistry, Graduate School of Science, Tohoku University, 6-3 Aramaki Aza Aoba, Aoba-ku, Sendai, Miyagi 980-8578, Japan. E-mail: mterada@tohoku.ac.jp

† Electronic supplementary information (ESI) available. See DOI: <https://doi.org/10.1039/d3sc01637d>

conformational changes, which often generate diverse TS variants. This increases computational complexity in evaluating whether the structural modification of a catalyst and/or substrate is suitable or not.⁴

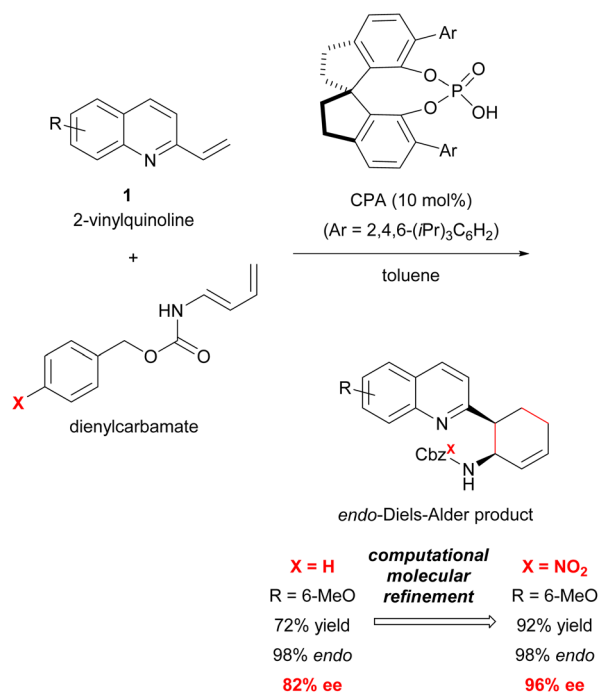
In contrast to the “distortion strategy”, the “interaction strategy” is aimed at stabilizing **major-TS** (Fig. 1, strategy B). The advantages of this strategy are that significant conformational changes in the TSs are unlikely to occur and, more importantly, that the stabilization of **major-TS** is expected to improve the reaction rate when the stereo-determining step is also the rate-determining step. However, the stabilization factors in **major-TS** are often difficult to predict visually because TS stability in enantioselective catalysis is determined by a delicate balance between the strain in the catalyst–substrate complex and the sum of weak interactions including hydrogen bonding, π -stacking, and dispersion interactions, as even relatively weak interactions can have a significant impact on the enantioselectivity.^{1a,5} Another issue to consider is whether a slight change in interaction energy could be precisely estimated by computational chemistry.⁶ Recently, Anderson *et al.*^{2b} and Hartwig *et al.*^{2c} have independently overcome this critical issue by computational design to reinforce metal– π interaction and dispersion interaction, respectively, to improve the enantioselectivity as well as the reaction rate.

Hydrogen bonding is a ubiquitous interaction that is universally used in the formation of organized molecular structures. It has also played an important role in the development of enantioselective reactions using not only organocatalysts⁷ but also transition metal catalysts.^{8,9} Because hydrogen bonding interaction, as broadly defined, is highly directional and electrostatic, it can be readily recognized visually; this allows the strength of the interaction to be controlled at the intended location by changing the electronic property around the bond. We envisioned the selective stabilization of **major-TS** by strengthening its hydrogen bonding interactions; it was anticipated that the enantioselectivity and the reaction rate would be improved efficiently without causing significant conformational changes in the TSs. This new methodology based on the “interaction strategy” using hydrogen bonding as the key interaction is expected to offer a versatile approach that will contribute to the development of a variety of catalytic enantioselective reactions.

Enantioselective catalysis using a chiral Brønsted acid has been a useful tool in organic synthesis.^{7,10} Since the introduction of 1,1'-bi-2-naphthol (BINOL)-derived chiral phosphoric acids (CPAs) as privileged chiral Brønsted acid catalysts,¹¹ continuous efforts have been devoted to achieving a broad range of unprecedented catalytic enantioselective reactions by improving the acidity and the chiral environment.^{12–14} Such catalytic enantioselective reactions have been achieved because the acid/base dual function of the monofunctional phosphate moiety of CPAs is able to strictly define substrate location through hydrogen bonding and other interactions. In addition, the pseudo- C_2 symmetry of CPAs has rendered the design of CPA derivatives using computational and machine learning approaches possible.^{2d,g,15}

Previous studies have shown that the stereochemical outcome of CPA-catalysed reactions is markedly affected by hydrogen bonds.^{11d,14d,16} We hypothesized that the selective enhancement of hydrogen bonding interactions in **major-TS** would improve the stereochemical outcome. To demonstrate the viability of this hypothesis, we adopted the CPA-catalysed Diels–Alder reaction of 2-vinylquinolines **1** with dienylcarbamates as a model reaction (Scheme 1).^{17,18} In the present reaction system, it is anticipated that both vinylquinolines **1** and dienylcarbamates are captured by CPA through hydrogen bonding interactions, and hence, the reaction would proceed under the chiral environment created by CPA.^{14c,19} In addition, the Diels–Alder reaction generally proceeds through a concerted fashion. This reaction profile limits the conformational flexibility of the corresponding TSs, and the rate enhancement is also expected by the intended strategy because the rate-determining step coincides with the stereo-determining step. Therefore, the proposed Diels–Alder reaction is an ideal system for verifying the “interaction strategy”.

Here we report the realization of the “interaction strategy,” which resulted in a marked improvement of the enantioselectivity and the reaction rate, by computational molecular refinement of dienylcarbamates. As the representative result shown in Scheme 1, a slight modification (*i.e.*, the introduction of an electron-withdrawing nitro group) to the benzene ring of the Cbz protecting group markedly enhanced the enantioselectivity. The molecular refinement was accomplished by a thorough analysis of the TS structures followed by adjustment of the strength of hydrogen bonds to enhance the interaction energy in the TS of the major reaction pathway. The present



Scheme 1 Model reaction for the “interaction strategy”: enantioselective Diels–Alder reaction of 2-vinylquinolines with dienylcarbamates catalysed by CPA.



approach provides a practical *in silico* molecular refinement strategy for enantioselective catalysis as well as a synthetic route to potentially useful quinoline derivatives in a highly *endo*- and enantioselective manner.²⁰

Results and discussion

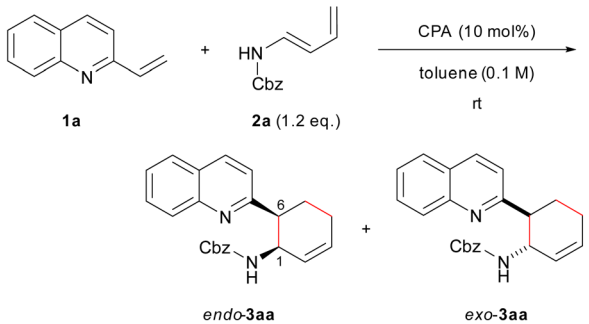
At the outset of our study, we conducted a brief screening of CPAs that could be used to realize the “interaction strategy”. The model reaction was performed using 2-vinylquinoline **1a** and dienylcarbamate **2a** under the influence of 10 mol% CPA catalyst in toluene at room temperature (Table 1). The use of typical BINOL-derived CPA catalysts (*R*)-**4a** and (*R*)-**4b** having 2,4,6-triisopropylphenyl and 9-anthryl groups, respectively, at the 3,3'-positions resulted in the complete consumption of **1a**, and desired product **3aa** was obtained in high yield (entries 1 and 2). On the other hand, (*R*)-**4c** having a 4-*t*Bu group was less effective (entry 3), affording **3aa** in moderate yield presumably because of catalyst deactivation. The *endo*-selectivity (80–90%) was not markedly influenced by the substituent introduced at

the 3,3'-positions of BINOL, whereas the enantioselectivity was highly dependent on the structural property of the introduced substituent (entries 1–3). Among typical substituents tested, the 2,4,6-triisopropylphenyl group displayed the highest enantioselectivity (entry 1: 71% ee for *endo*-**3aa**). To enhance the enantioselectivity, the catalyst chiral backbone was further investigated using 2,4,6-triisopropylphenyl substituted catalysts (entries 4 and 5); *endo*-**3aa** was obtained exclusively with high enantioselectivity, albeit in moderate yield, when SPINOL-derived (*S*)-**6** was used (entry 5). Because of the partial hydrolysis of dienylcarbamate **2a** during the course of the reaction, MS 5A was added (entry 6), affording (1*R*,6*S*)-*endo*-**3aa** as the major enantiomer in high yield with slightly improved enantioselectivity (92% ee) (see Table S1† for details). The relative and absolute stereochemistry of **3aa** was determined by the derivatization of **3aa** into a stereochemically known compound (see ESI† for details).

The main goal of this study was to realize the intended “interaction strategy” based on the initial reaction system identified by the brief screening of CPAs. To investigate the interaction mode between catalyst (*S*)-**6** and substrates (**1a** and **2a**) in the TSs, we thoroughly explored the favourable TSs for each enantiomer of *endo*-**3aa**. Structure searches were manually performed by primarily changing the conformation of the Cbz group: the orientation of the benzyl moiety and the geometry of the carbamate unit, *i.e.*, *s-cis* and *s-trans*, because, in general, the Diels–Alder reaction proceeds through a concerted fashion and hence the simultaneous formation of the two carbon–carbon bonds restricts the flexibility of the relative location between dienophile **1a** and diene **2a**. As shown in Fig. 2 and schematic models in Table 2, **TS_R(H)** and **TS_S(H)** for the formation of major enantiomer (1*R*,6*S*)-*endo*-**3aa** and the minor one, respectively, were optimized by DFT calculations at the M06-2X/6-31g(d) level of theory in gas phase (Tables S2 and S3† for details).²¹ As expected, both dienophile **1a** and diene **2a** were fixed in the appropriate positions by the phosphoric acid unit of catalyst (*S*)-**6** primarily through hydrogen bonding (N¹...H¹...O¹ and N²...H²...O²) in stable **TS_R(H)** and **TS_S(H)** (see schematic models shown in Table 2). **TS_R(H)**, which led to (1*R*,6*S*)-*endo*-**3aa**, was energetically more favorable than **TS_S(H)** at 1.8 kcal mol^{−1} (calcd: 91% ee); this was in good agreement with the experimental value (observed: 92% ee) and the absolute stereochemistry obtained. In addition, the results of IRC calculations suggested that the present Diels–Alder reaction proceeds through an asynchronous concerted pathway rather than a stepwise mechanism.²²

We conducted the distortion/interaction analysis of **TS_R(H)** and **TS_S(H)** (see Table S4† for details),^{3,16f,23} followed by a detailed analysis of characteristic interactions, in particular, hydrogen bonding interactions and their energies. As shown in Fig. 2, the conformation of the Cbz protecting group of dienylcarbamate **2a** is completely different. In **TS_R(H)**, the benzyl moiety of the Cbz group and the carbamate unit are coplanar, whereas in **TS_S(H)**, the benzyl moiety is oriented outside the plane formed by the carbamate unit. As summarized in Table 2, the detailed comparison between the respective TSs revealed marked differences in some of the interactions in terms of not

Table 1 Initial screening of CPAs^a



(R)-**4a** (Ar = 2,4,6-*i*Pr₃C₆H₂) (R)-**5** (Ar = 2,4,6-*i*Pr₃C₆H₂) (S)-**6** (Ar = 2,4,6-*i*Pr₃C₆H₂)
 (R)-**4b** (Ar = 9-anthryl)
 (R)-**4c** (Ar = 4-*t*BuC₆H₄)

Entry	CPA	Time (h)	Yield of 3aa ^b (%)	<i>endo</i> / <i>exo</i> ^c	ee ^c (%)
1	(<i>R</i>)- 4a	12	95	81 : 19	71/88
2	(<i>R</i>)- 4b	36	95	88 : 12	5/−12
3	(<i>R</i>)- 4c	36	67	87 : 13	5/−3
4	(<i>R</i>)- 5	20	95	74 : 26	71/ND ^d
5	(<i>S</i>)- 6	74	62	99 : 1	88/ND ^d
6 ^e	(<i>S</i>)- 6	5 d	91	99 : 1	92/ND ^d

^a Unless otherwise noted, all reactions were carried out using 0.1 mmol of **1a**, 0.12 mmol of **2a**, and 0.010 mmol of CPA catalyst (10 mol%) in toluene (1 mL). ^b Isolated yield. ^c Diastereomeric and enantiomeric excess were determined by chiral stationary phase HPLC analysis. ^d ND: not determined. ^e MS 5A (50 mg) was used as an additive.



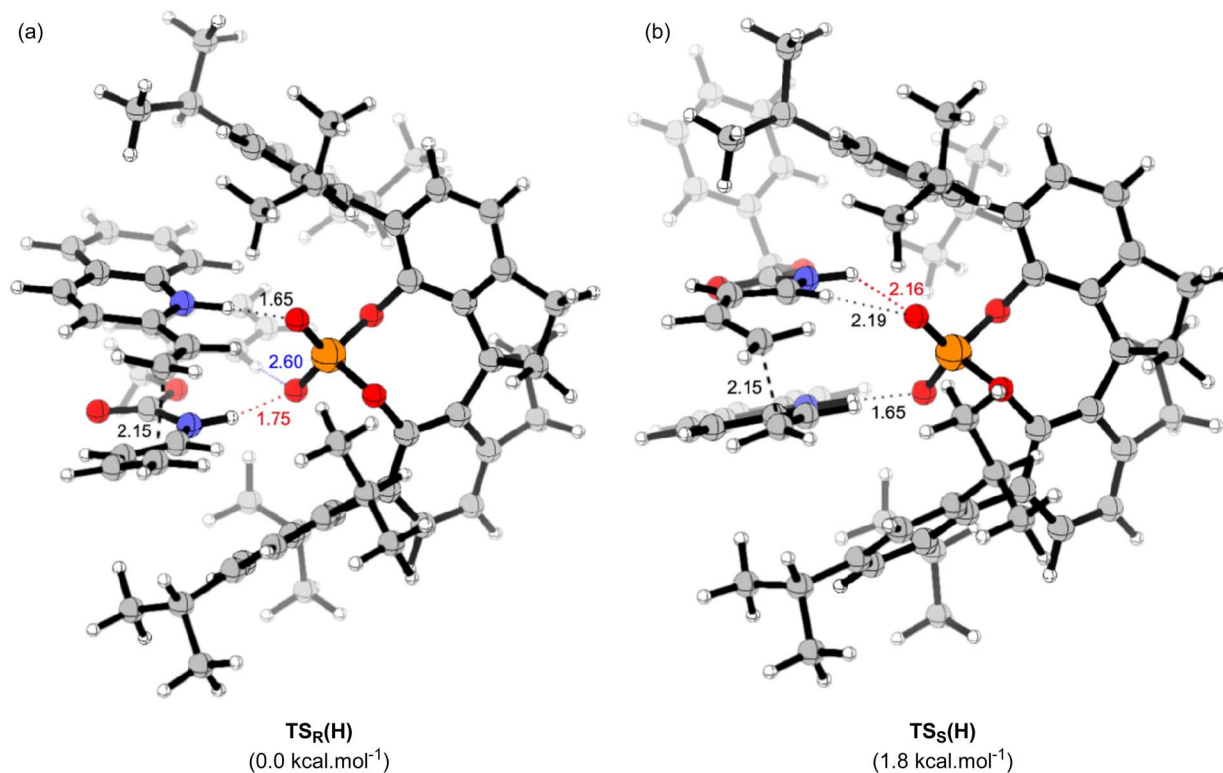
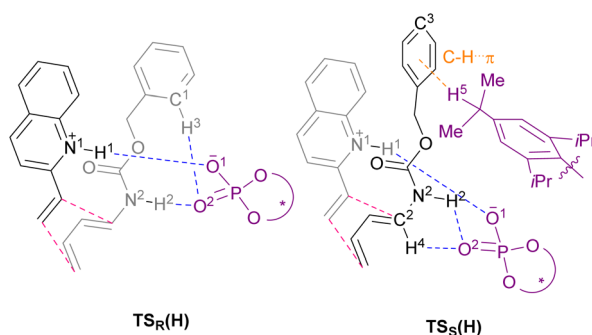


Fig. 2 Optimized transition state structures for the *endo* addition. Relative free energies are shown in parentheses. The transition state structures were fully optimized using the M06-2X/6-31g(d) level of theory in gas phase. (a) Transition state for the formation of (1*R*,6*S*)-*endo*-3aa. (b) Transition state for the formation of (1*S*,6*R*)-*endo*-3aa.

Table 2 Schematic models of TS_R(H) and TS_S(H) and the summary of hydrogen bonding interactions



Hydrogen bond	<i>L</i> : length (Å), <i>A</i> : angle (°), <i>E</i> : energy (kcal mol ⁻¹)	TS _R (H)	TS _S (H)
N ¹ ...H ¹ ...O ¹	<i>L</i> (H ¹ -O ¹)	1.65	1.65
	<i>A</i> (N ¹ -H ¹ -O ¹)	169	171
	<i>E</i> (H ¹ -O ¹)	13.3	12.8
N ² ...H ² ...O ²	<i>L</i> (H ² -O ²)	1.75	2.16
	<i>A</i> (N ² -H ² -O ²)	167	123
	<i>E</i> (H ² -O ²)	10.4	1.3
C ¹ -H ³ ...O ²	<i>L</i> (H ³ -O ²)	2.60	—
	<i>A</i> (C ¹ -H ³ -O ²)	167	—
	<i>E</i> (H ³ -O ²)	0.8	—
C ² -H ⁴ ...O ²	<i>L</i> (H ⁴ -O ²)	—	2.19
	<i>A</i> (C ² -H ⁴ -O ²)	—	123
	<i>E</i> (H ⁴ -O ²)	—	2.4
C-H ⁵ ...C ³	<i>L</i> (H ⁵ -C ³)	—	2.82

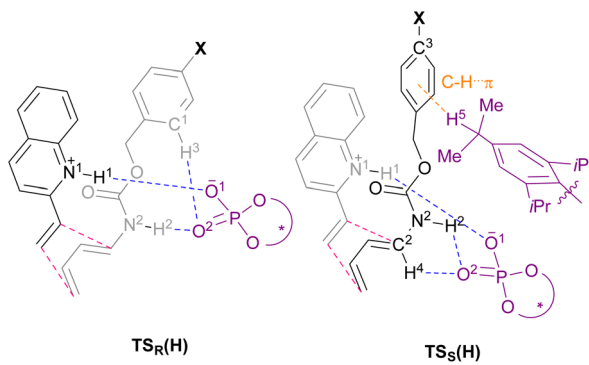


only the energy but also the site of hydrogen bonds. The strength of the hydrogen bonds was estimated using NBO calculations.²⁴ The interaction energy of the hydrogen bond ($H^1 \cdots O^1$) formed between dienophile **1a** (N^1-H^1) and CPA ($O^1=P$) was comparable between the two states [$TS_R(H)$: 13.3 kcal mol⁻¹ vs. $TS_S(H)$: 12.8 kcal mol⁻¹] presumably because it is the key interaction to activate dienophile **1a** (*i.e.*, through protonation) [$L(H^1-O^1) = 1.65$ Å for both $TS_R(H)$ and $TS_S(H)$]. In contrast, the hydrogen bond ($H^2 \cdots O^2$) formed between dienylcarbamate (N^2-H^2) and CPA ($O^2=P$) was significantly shorter in $TS_R(H)$ than in $TS_S(H)$ [$L(H^2-O^2) = 1.75$ Å vs. 2.16 Å]. In addition, the three atoms (N^2 , H^2 , and O^2) involved in hydrogen bonding formed an almost straight line in $TS_R(H)$ [$\angle(N^2-H^2-O^2) = 167^\circ$], whereas in $TS_S(H)$, the corresponding bond formed a bent structure [$\angle(N^2-H^2-O^2) = 123^\circ$]. Reflecting these differences in bond length and angle, the interaction energy of the hydrogen bond ($H^2 \cdots O^2$) in $TS_R(H)$ (10.4 kcal mol⁻¹) was markedly higher than that in $TS_S(H)$ (1.3 kcal mol⁻¹). The significant difference in interaction energy appeared to contribute to the high enantioselectivity. More interestingly, in $TS_R(H)$, *ortho* C^1-H^3 of the phenyl ring in the Cbz group formed a hydrogen bond with the phosphoryl oxygen of CPA ($O^2=P$), although its interaction energy was small [$E(H^3-O^2) = 0.8$ kcal mol⁻¹]. In contrast, in $TS_S(H)$, other bonds were formed between dienylcarbamate (C^2-H^4) and CPA ($O^2=P$) [$E(H^4-O^2) = 2.4$ kcal mol⁻¹], as well as between the catalyst substituent ($C-H^5$) and the π orbital of the phenyl ring in the Cbz group (Fig. S2†).

We then moved on to redesign the substrates to further enhance the enantioselectivity, which is the core of the present study. The detailed analysis of the TSs revealed that, in $TS_R(H)$ and $TS_S(H)$, different hydrogen bonds were formed between the Cbz protecting group of dienylcarbamate **2a** and CPA (*S*)-**6**: in $TS_R(H)$, C-H \cdots O interaction occurred between *ortho* C^1-H^3 of the Cbz phenyl ring and CPA ($O^2=P$), whereas in $TS_S(H)$, C-H \cdots π interaction occurred between the isopropyl group of the CPA substituent ($C-H^5$) and the Cbz phenyl ring (Table 2 and Fig. 2). These findings led us to hypothesize that the intended “interaction strategy” might be accomplished through the modification of the phenyl ring of the Cbz moiety, *i.e.*, the protective group of the nitrogen atom of **2a**. When the electron density of the Cbz phenyl ring is reduced by the introduction of an electron-withdrawing group (EWG), an increase in the hydrogen bonding interaction ($C^1-H^3 \cdots O^2$) owing to the enhancement of the acidity of C^1-H^3 is anticipated only in $TS_R(H)$. Consequently, the hydrogen bond ($H^3 \cdots O^2$) stabilizes $TS_R(H)$, *i.e.*, the TS of the major reaction pathway, but not $TS_S(H)$. The modification of the Cbz phenyl ring by the introduction of an EWG is thus predicted to result in increased enantioselectivity.²⁵

In order to confirm the above hypothesis, we calculated the TSs of the Diels–Alder reaction between dienophile **1a** and dienylcarbamates having a bromo group (**7a**: X = Br) or a nitro group (**8a**: X = NO₂) as an EWG at the *para*-position of the Cbz phenyl ring. Characteristic hydrogen bonds in these TSs are summarized in Table 3 [the structures of $TS_R(Br)/TS_S(Br)$ for the reaction of **1a** with **7a** and $TS_R(NO_2)/TS_S(NO_2)$ for the reaction of **1a** with **8a** are shown in Fig. S3 and S4,† respectively]. As

Table 3 Schematic models for $TS_R(X)$ and $TS_S(X)$ and summary of hydrogen bonding interactions in the TSs of the Diels–Alder reaction of parent **2a** (X = H) with redesigned dienylcarbamates **7a** (X = Br) and **8a** (X = NO₂)



	$TS_R(H)$	$TS_R(Br)$	$TS_R(NO_2)$	$TS_S(H)$	$TS_S(Br)$	$TS_S(NO_2)$
<i>L</i> : length (Å),						
<i>A</i> : angle (°)						
<i>L</i> (H^1-O^1)	1.65	1.65	1.64	1.65	1.65	1.64
<i>A</i> ($N^1-H^1-O^1$)	169	170	170	171	171	171
<i>E</i> (H^1-O^1)	13.3	13.7	13.9	12.8	12.5	12.8
<i>L</i> (H^2-O^2)	1.75	1.76	1.76	2.16	2.17	2.14
<i>A</i> ($N^2-H^2-O^2$)	167	165	165	123	123	124
<i>E</i> (H^2-O^2)	10.4	9.9	10.0	1.3	1.2	1.4
<i>L</i> (H^3-O^2)	2.60	2.37	2.31	—	—	—
<i>A</i> ($C^1-H^3-O^2$)	167	168	172	—	—	—
<i>E</i> (H^3-O^2)	0.8	1.8	2.3	—	—	—
<i>L</i> (H^4-O^2)	—	—	—	2.19	2.17	2.19
<i>A</i> ($C^2-H^4-O^2$)	—	—	—	123	124	122
<i>E</i> (H^4-O^2)	—	—	—	2.4	2.6	2.4
<i>L</i> (H^5-C^3)	—	—	—	2.82	2.81	2.76

expected, neither **7a** nor **8a** displayed significant changes in the TS structures compared with those of parent dienylcarbamate **2a** (X = H) (Table 3 and Fig. 2 vs. Fig. S3 and S4†). Specifically, almost no differences in hydrogen bond length and angle were observed in $TS_S(X)$ (X = H, Br, or NO₂). In contrast, the detailed analysis of $TS_R(X)$ structure revealed that the length of the hydrogen bond formed between the Cbz phenyl ring of dienylcarbamate (C^1-H^3) and CPA ($O^2=P$) tended to become shorter [$L(H^3-O^2)$ (Å), X = H: 2.60 → Br: 2.37 → NO₂: 2.31] with increasing electron-withdrawing nature of the substituent (Hammett σ_m constants, X = H: 0.0 → Br: +0.393 → NO₂: +0.710).²⁶

The introduction of an EWG to the Cbz phenyl ring decreases the electron density of the proton H^3 , making the hydrogen bonding interaction stronger and the bond length shorter. Indeed, as shown in Table 4, the electron density around H^3 decreased [$P(H^3)$, X = H: 0.7188 → Br: 0.7073 → NO₂: 0.7016] with an increase in the electron-withdrawing nature of the substituent. NBO calculations revealed that the interaction energy of the hydrogen bond ($H^3 \cdots O^2$) in $TS_R(X)$ was enhanced gradually [$E(H^3-O^2)$ (kcal mol⁻¹), X = H: 0.8 → Br: 1.8 → NO₂: 2.3] and more importantly, $\Delta\Delta G^\ddagger$ markedly improved [$\Delta\Delta G^\ddagger$ (kcal mol⁻¹), X = H: 1.8 → Br: 2.0 → NO₂: 3.0]. On the basis of these calculation results, we predicted that the introduction of



Table 4 Characteristics of the hydrogen bond ($\text{H}^3 \cdots \text{O}^2$) in $\text{TS}_R(\text{X})$ for the formation of the major enantiomer

X	σ_m	$L(\text{H}^3-\text{O}^2)$ (Å)	$P(\text{H}^3)^a$	$E(\text{H}^3-\text{O}^2)^b$	$\Delta\Delta G^\ddagger$	Calcd ee (%)
2a: H	0.0	2.60	0.7188	0.8	1.8	91
7a: Br	+0.393	2.37	0.7073	1.8	2.0	94
8a: NO_2	+0.710	2.31	0.7016	2.3	3.0	99

^a By natural population analysis. ^b In kcal mol^{-1} .

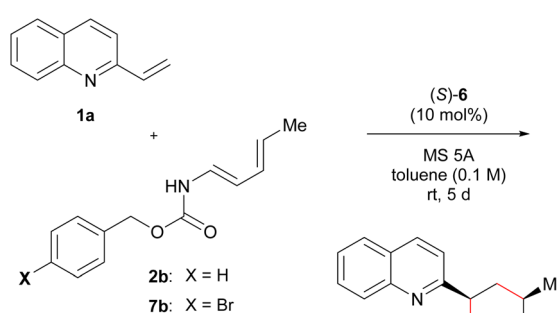
an EWG at the *para*-position of the Cbz phenyl ring would result in increased enantioselectivity, and hence, the intended “interaction strategy” could improve the enantioselectivity of the present Diels–Alder reaction.

To verify our calculation results, a series of dienylcarbamates **2b** and **7b–10b** having electronically different substituents X were tested in the reaction of **1a** catalysed by (*S*)-**6a**. As shown in Table 5, the intended “interaction strategy” was achieved: the enantioselectivity improved with the introduction of stronger electron-withdrawing substituents [$\text{X} = \text{H}$ (**2b**): 91% ee \rightarrow Br (**7b**): 95% ee \rightarrow NO_2 (**8b**): 98% ee], as predicted by the calculations. When dienylcarbamate **8b** having a nitro group²⁷ was applied to the reaction, a large improvement in enantioselectivity (98% ee) was observed compared with when parent dienylcarbamate **2b** (91% ee) was used. Since this modification

site is far from the reaction site *i.e.*, the diene moiety, these improvements in enantioselectivities could only be achieved by computational predictions, otherwise it is extremely difficult to find an appropriate modification method and site of the substrate through experimental exploration.

On the other hand, no significant difference in enantioselectivity (90% ee) was observed when electron-donating substituents such as methyl (**9b**) and methoxy (**10b**) groups were introduced at the *para*-position of the Cbz phenyl ring. Fig. 3 shows the Hammett plot of σ_m constants vs. $\Delta\Delta G^\ddagger$, which were calculated from enantioselectivities obtained experimentally. Generally, a nearly linear correlation was observed with only the methoxy substituent slightly deviating from this relationship. This discrepancy is likely attributed to the electron-donating methoxy substituent enhancing the $\text{C}-\text{H} \cdots \pi$ interaction in $\text{TS}_S(\text{MeO})$,²⁸ *i.e.*, the TS of the minor reaction pathway. Consequently, $\text{TS}_S(\text{MeO})$ was stabilized, and hence, the reduction of enantioselectivity was estimated. However, the inductive effect of the methoxy group at the *meta*-position (Hammett σ_m constants, $\text{X} = \text{MeO}$: +0.115)²⁶ could stabilize $\text{TS}_R(\text{MeO})$, *i.e.*, the TS of the major reaction pathway, through the hydrogen bond ($\text{H}^3 \cdots \text{O}^2$). It is thus presumed that the stabilization of $\text{TS}_S(\text{MeO})$ by the $\text{C}-\text{H} \cdots \pi$ interaction counterbalanced the stabilization of $\text{TS}_R(\text{MeO})$ by the hydrogen bond ($\text{H}^3 \cdots \text{O}^2$), making the enantioselectivity of **14ab** ($\text{X} = \text{MeO}$) comparable to that of **3ab** ($\text{X} = \text{H}$).

Next, we investigated the generality of the “interaction strategy” in the reactions of a series of vinylquinolines **1** with redesigned dienylcarbamates **8** ($\text{X} = \text{NO}_2$) having a nitro group

Table 5 Validation of the substituent effect in the reaction of **1a** with a series of dienylcarbamates^a


Entry	X	Product	Yield ^b (%)	<i>endo/exo</i> ^c	ee ^c (%)
1	H (2b)	3ab (Cbz)	86	98 : 2	91
2	Br (7b)	11ab (Cbz ^{Br})	98	98 : 2	95
3	NO_2 (8b)	12ab (Cbz ^{NO_2})	98	99 : 1	98
4	Me (9b)	13ab (Cbz ^{Me})	85	98 : 2	90
5	MeO (10b)	14ab (Cbz ^{MeO})	95	98 : 2	90

^a General conditions: **1a** (0.1 mmol), dienylcarbamate (0.3 mmol), and (*S*)-**6** (0.01 mmol) in toluene (1 mL) with MS 5A (50 mg) at room temperature for 5 days. ^b Isolated yield. ^c Diastereomeric and enantiomeric excess were determined by chiral stationary phase HPLC analysis.

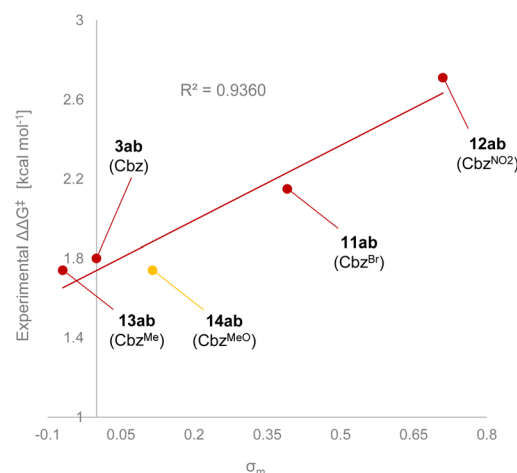
**Fig. 3** Hammett plot of $\Delta\Delta G^\ddagger$ vs. σ_m constants.

Table 6 Generality of the “interaction strategy” using a series of substrates^a

$(S)\text{-}6$
 (10 mol%)
 MS 5A
 toluene (0.1 M)
 rt

	8 (X = NO ₂) or 2 (X = H)	12 (X = NO ₂) or 3 (X = H)	
1		12aa (X = NO ₂) 99% yield 99% <i>endo</i> 98% ee	3aa (X = H) 91% yield 99% <i>endo</i> 92% ee
2		12ba (X = NO ₂) 99% yield 99% <i>endo</i> 99% ee	3ba (X = H) 95% yield 98% <i>endo</i> 93% ee
3		12ca (X = NO ₂) 92% yield 98% <i>endo</i> 96% ee	3ca^b (X = H) 72% yield 98% <i>endo</i> 82% ee
4		12da (X = NO ₂) 97% yield 99% <i>endo</i> 98% ee	3da (X = H) 97% yield 99% <i>endo</i> 86% ee
5		12ea (X = NO ₂) 96% yield 99% <i>endo</i> 98% ee	3ea^b (X = H) 63% yield >99% <i>endo</i> 85% ee
6		12fa (X = NO ₂) 86% yield 99% <i>endo</i> 99% ee	3fa (X = H) 83% yield 99% <i>endo</i> 91% ee
7		12ga (X = NO ₂) 99% yield 98% <i>endo</i> 98% ee	3ga^b (X = H) 96% yield 98% <i>endo</i> 87% ee
8		12ha (X = NO ₂) 85% yield 98% <i>endo</i> 92% ee	3ha^b (X = H) 79% yield 98% <i>endo</i> 49% ee
9 ^c		12ac (X = NO ₂) 94% yield 97% <i>endo</i> 95% ee	3ac (X = H) 89% yield 98% <i>endo</i> 93% ee
10		12ad (X = NO ₂) 98% yield >99% <i>endo</i> 99% ee	3ad (X = H) 87% yield 99% <i>endo</i> 96% ee

^a General conditions: **1** (0.1 mmol), **8** (or **2**) (0.12 mmol), and (*S*)-**6** (0.01 mmol) in toluene (1 mL) with MS 5A (50 mg) at room temperature for 5 days. ^b 7 days. ^c 3.0 eq. of **8** (or **2**) was used.

on the Cbz phenyl ring. As shown in Table 6, all substrates tested underwent the reactions smoothly, affording corresponding products **endo**-**12** (X = NO₂) exclusively in high chemical yields with improved enantioselectivities compared with when parent dienylcarbamates **2** (X = H) having the normal Cbz group were used. In fact, investigation of the substituent effect of a variety of vinylquinolines **1** revealed that the use of redesigned dienylcarbamate **8a** facilitated the reactions (entries 1–8). Corresponding products **12** were obtained in high yields with extremely high enantioselectivities, regardless of the electronic nature or position of the substituent introduced to the quinoline ring. In particular, the enantioselectivity in the reaction of vinylquinoline **1h** having a chloride substituent at the 7-position with redesigned dienylcarbamate **8a** was markedly improved (92% ee) compared with the enantioselectivity in the reaction of **1h** with parent dienylcarbamate **2a** (49% ee) (entry 8). Furthermore, the use of dienylcarbamates **8c** (R² = *n*Bu, R³ = H) and **8d** (R² = H, R³ = Me), whose substituents and substitution pattern differ from those of **8b** (R² = Me, R³ = H), respectively, also resulted in increases in both yield and enantioselectivity (entries 9 and 10).

Finally, we performed a kinetic analysis to determine whether a marked improvement in the enantioselectivities of **12** could be achieved by the intended “interaction strategy” (Fig. 4). If the improvement of enantioselectivity stems from the stabilization of the TS of the major reaction pathway, the use of redesigned dienylcarbamates **8** is expected to enhance the rate of the present reaction, *i.e.*, a normal electron demand Diels–

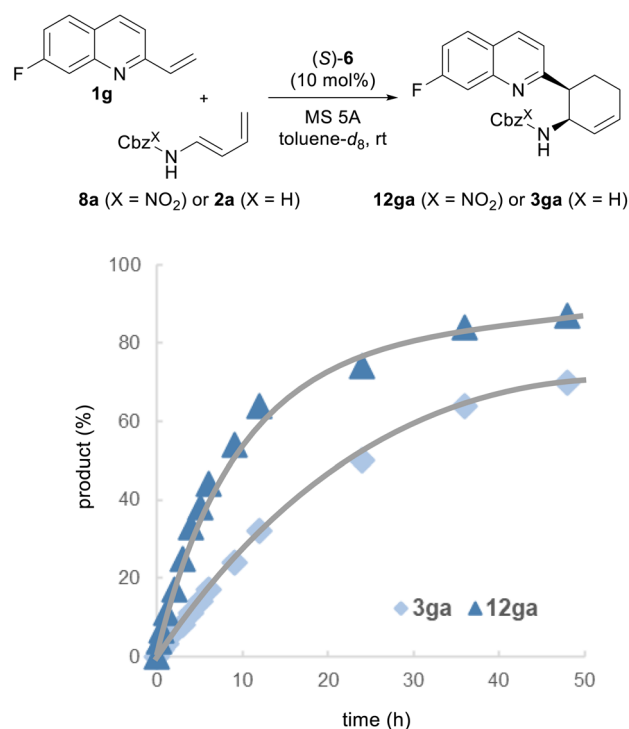


Fig. 4 ¹H and ¹⁹F NMR experiments. Reaction conditions: **1g** (0.05 mmol), **2a** or **8a** (0.06 mmol, 1.2 eq.), (*S*)-**6** (10 mol%) and activated MS 5A (10 mg) in toluene-*d*₈ at room temperature for 48 h. CH₂Br₂ and C₆H₅CF₃ were used as internal standards.



Alder reaction, despite the introduction of the electron-withdrawing nitro substituent to the diene subunit.^{2b,c,29} This prediction is also supported by the calculated activation free energy (ΔG^\ddagger): ΔG^\ddagger of $\text{TS}_\text{R}(\text{NO}_2)$ in the reaction of **8a** with **1a** [$\text{TS}_\text{R}(\text{NO}_2)$: 9.4 kcal mol⁻¹] is lower than that of $\text{TS}_\text{R}(\text{H})$ in the reaction of **2a** with **1a** [$\text{TS}_\text{R}(\text{H})$: 10.1 kcal mol⁻¹] (Fig. S1†). Moreover, because $\text{TS}_\text{R}(\text{NO}_2)$ and $\text{TS}_\text{R}(\text{H})$ have the highest energy barrier, the pathway involving these TSs is the rate-determining step, and consequently, the stereo-determining step is also the rate-determining step. With these considerations in mind, we conducted kinetic studies on the reaction of **1g** with redesigned **8a** catalyzed by (*S*)-**6** and compared the results with those of the reaction of **1g** with parent **2a**. The progress of the reaction was monitored by ¹H NMR and ¹⁹F NMR measurements. As predicted, the reaction rate was clearly higher with redesigned **8a** than with parent **2a**. These results prove that the intended “interaction strategy” is successful and confirm the validity of our molecular design.

Conclusions

We have demonstrated the enantioselective Diels–Alder reaction of 2-vinylquinolines with dienylcarbamates as a model reaction under the influence of CPA catalyst in accordance with the “interaction strategy”. In the development of enantioselective catalysis, computational studies have aided in the design of catalyst molecules and reaction systems in recent years. Among computational approaches reported thus far, the “interaction strategy”, which focuses on the stabilization of the TS of the major reaction pathway to improve enantioselectivity, has largely been unexplored despite the marked advantages of the intended strategy. In order to realize the “interaction strategy”, we envisaged the effective use of hydrogen bonding interactions. Indeed, the hydrogen bonding interactions made a significant impact on not only the enantioselectivity but also the reaction rate and are useful in refining reaction systems. Particularly, in the present molecular refinement aided by the computational studies, these achievements could only be realized by computational predictions, otherwise it is difficult to find out the modification site through experimental explorations because the modified site of the Cbz group is located far from the reaction site. More importantly, the improvement of enantioselectivity is anticipated by applying the present strategy not only to the most stable TS, but also to the second or third most stable TS. This is because the reinforced hydrogen bonding interaction may also reverse the order of stability between these TSs. This new methodology based on the “interaction strategy” using hydrogen bonding as the key interaction is a versatile “*in silico*” approach that will contribute to the refinement of a variety of catalytic enantioselective reactions. Further application of the “interaction strategy” is in progress to develop efficient and distinctive enantioselective reactions using not only CPA catalysts but also organocatalysts and transition metal catalysts.

Data availability

The exploratory investigation, experimental procedures, computational data, and characterization data are available.

Author contributions

T. N. contributed conceptualization, design of the work, data curation, formal analysis, investigation (experimental and theoretical studies), and writing – original draft. M. T. contributed conceptualization, project administration, writing – review & editing, supervision, and funding acquisition.

Conflicts of interest

There are no conflicts to declare.

Acknowledgements

The computation was performed using Research Center for Computational Science, Okazaki, Japan (Project: 22-IMS-C127). This work was supported by a Grant-in-Aid for Scientific Research on Innovative Areas “Hybrid Catalysis for Enabling Molecular Synthesis on Demand” (JP17H06447) from MEXT, Japan (M. T.), a Grant-in-Aid for Challenging Research (Exploratory) (JP22K19018) from JSPS (M. T.), and a Grant-in-Aid for Young Scientists (JP21J14551) from JSPS, Japan (T. N.).

Notes and references

- For selected reviews, see: (a) S. E. Wheeler, T. J. Seguin, Y. Guan and A. C. Doney, *Acc. Chem. Res.*, 2016, **49**, 1061–1069; (b) Q. Peng, F. Duarte and R. S. Paton, *Chem. Soc. Rev.*, 2016, **45**, 6093–6107; (c) J. P. Reid and M. S. Sigman, *Nat. Rev. Chem.*, 2018, **2**, 290–305; (d) D. Ess, L. Gagliardi and S. Hammes-Schiffer, *Chem. Rev.*, 2019, **119**, 6507–6508; (e) S. Ahn, M. Hong, M. Sundararajan, D. H. Ess and M.-H. Baik, *Chem. Rev.*, 2019, **119**, 6509–6560; (f) P. Nakliang, S. Yoon and S. Choi, *Org. Chem. Front.*, 2021, **8**, 5165–5181.
- (a) G. Jindal and R. B. Sunoj, *Org. Biomol. Chem.*, 2014, **12**, 2745–2753; (b) R. N. Straker, Q. Peng, A. Mekareeya, R. S. Paton and E. A. Anderson, *Nat. Commun.*, 2016, **7**, 10109; (c) H. Iwamoto, T. Imamoto and H. Ito, *Nat. Commun.*, 2018, **9**, 2290; (d) S.-S. Meng, P. Yu, Y.-Z. Yu, Y. Liang, K. N. Houk and W.-H. Zheng, *J. Am. Chem. Soc.*, 2020, **142**, 8506–8513; (e) Y. Xi, B. Su, X. Qi, S. Pedram, P. Liu and J. F. Hartwig, *J. Am. Chem. Soc.*, 2020, **142**, 18213–18222; (f) A. Hamza, K. Sorochkina, B. Kótai, K. Chernichenko, D. Berta, M. Bolte, M. Nieger, T. Repo and I. Pápai, *ACS Catal.*, 2020, **10**, 14290–14301; (g) M. Duan, C. D. Díaz-Oviedo, Y. Zhou, X. Chen, P. Yu, B. List, K. N. Houk and Y. Lan, *Angew. Chem., Int. Ed.*, 2022, **61**, e202113204.
- F. M. Bickelhaupt and K. N. Houk, *Angew. Chem., Int. Ed.*, 2017, **56**, 10070–10086.
- (a) A. C. Doney, B. J. Rooks, T. Lu and S. E. Wheeler, *ACS Catal.*, 2016, **6**, 7948–7955; (b) L. C. Burrows, L. T. Jesikiewicz, G. Lu, S. J. Geib, P. Liu and K. M. Brummond, *J. Am. Chem. Soc.*, 2017, **139**, 15022–15032.
- (a) R. R. Knowles and E. N. Jacobsen, *Proc. Natl. Acad. Sci. U. S. A.*, 2010, **107**, 20678–20685; (b) R. J. Phipps, *Synlett*, 2016,



- 27, 1024–1026; (c) C. R. Kennedy, S. Lin and E. N. Jacobsen, *Angew. Chem., Int. Ed.*, 2016, **55**, 12596–12624; (d) W. Yan, M. Zheng, C. Xu and F.-E. Chen, *Green Synthesis and Catalysis*, 2021, **2**, 329–336.
- 6 R. Huber, A. Passera, E. Gubler and A. Mezzetti, *Adv. Synth. Catal.*, 2018, **360**, 2900–2913.
- 7 For reviews, see: (a) M. S. Taylor and E. N. Jacobsen, *Angew. Chem., Int. Ed.*, 2006, **45**, 1520–1543; (b) A. G. Doyle and E. N. Jacobsen, *Chem. Rev.*, 2007, **107**, 5713–5743; (c) X. Yu and W. Wang, *Chem.-Asian J.*, 2008, **3**, 516–532; (d) M. J. Ajitha and K.-W. Huang, *Synthesis*, 2016, **48**, 3449–3458.
- 8 (a) K. T. Mahmudov, A. V. Gurbanov, F. I. Guseinov and M. F. C. Guedes da Silva, *Coord. Chem. Rev.*, 2019, **387**, 32–46; (b) A. Fanourakis, P. J. Docherty, P. Chuentragool and R. J. Phipps, *ACS Catal.*, 2020, **10**, 10672–10714.
- 9 (a) P. Fackler, C. Berthold, F. Voss and T. Bach, *J. Am. Chem. Soc.*, 2010, **132**, 15911–15913; (b) M. C. Schwarzer, A. Fujioka, T. Ishii, H. Ohmiya, S. Mori and M. Sawamura, *Chem. Sci.*, 2018, **9**, 3484–3493; (c) K. Imai, Y. Takayama, H. Murayama, H. Ohmiya, Y. Shimizu and M. Sawamura, *Org. Lett.*, 2019, **21**, 1717–1721; (d) H. Murayama, Y. Heike, K. Higashida, Y. Shimizu, N. Yodsin, Y. Wongnongwa, S. Jungsuttiwong, S. Mori and M. Sawamura, *Adv. Synth. Catal.*, 2020, **362**, 4655–4661; (e) C.-T. Chen, Y.-C. Su, C.-H. Lu, C.-I. Lien, S.-F. Hung, C.-W. Hsu, R. Agarwal, R. Modala, H.-M. Tseng, P.-X. Tseng, R. Fujii, K. Kawashima and S. Mori, *ACS Catal.*, 2021, **11**, 7160–7175; (f) S. Sakai, A. Fujioka, K. Imai, K. Uchiyama, Y. Shimizu, K. Higashida and M. Sawamura, *Adv. Synth. Catal.*, 2022, **364**, 2333–2339.
- 10 For reviews on chiral Brønsted acid catalysis, see: (a) T. Akiyama, *Chem. Rev.*, 2007, **107**, 5744–5758; (b) D. Kampen, C. M. Reisinger and B. List, *Top. Curr. Chem.*, 2010, **291**, 395–456; (c) T. Akiyama and K. Mori, *Chem. Rev.*, 2015, **115**, 9277–9306; (d) T. James, M. van Gemmeren and B. List, *Chem. Rev.*, 2015, **115**, 9388–9409.
- 11 For reviews on BINOL-derived phosphoric acids and derivatives, see: (a) M. Terada, *Chem. Commun.*, 2008, 4097–4112; (b) M. Terada, *Synthesis*, 2010, 1929–1982; (c) D. Parmar, E. Sugiono, S. Raja and M. Rueping, *Chem. Rev.*, 2014, **114**, 9047–9153; (d) R. Maji, S. C. Mallonjjala and S. E. Wheeler, *Chem. Soc. Rev.*, 2018, **47**, 1142–1158; (e) B.-C. Da, S.-H. Xiang and B. Tan, *Chin. J. Chem.*, 2021, **39**, 1787–1796; For seminal studies of chiral phosphoric acid catalysts, see: (f) T. Akiyama, J. Itoh, K. Yokota and K. Fuchibe, *Angew. Chem., Int. Ed.*, 2004, **43**, 1566–1568; (g) D. Uraguchi and M. Terada, *J. Am. Chem. Soc.*, 2004, **126**, 5356–5357.
- 12 For selected examples on chiral phosphoric acids and phosphate in photoredox reactions, see: (a) L. J. Rono, H. G. Yayla, D. Y. Wang, M. F. Armstrong and R. R. Knowles, *J. Am. Chem. Soc.*, 2013, **135**, 17735–17738; (b) E. C. Gentry, L. J. Rono, M. E. Hale, R. Matsuura and R. R. Knowles, *J. Am. Chem. Soc.*, 2018, **140**, 3394–3402; (c) R. S. J. Proctor, H. J. Davis and R. J. Phipps, *Science*, 2018, **360**, 419–422; (d) N. Y. Shin, J. M. Ryss, X. Zhang, S. J. Miller and R. R. Knowles, *Science*, 2019, **366**, 364–369; (e) C. B. Roos, J. Demaerel, D. E. Graff and R. R. Knowles, *J. Am. Chem. Soc.*, 2020, **142**, 5974–5979; (f) A. S. K. Lahdenperä, P. D. Bacos and R. J. Phipps, *J. Am. Chem. Soc.*, 2022, **144**, 22451–22457.
- 13 L. Schreyer, R. Properzi and B. List, *Angew. Chem., Int. Ed.*, 2019, **58**, 12761–12777.
- 14 (a) D. Nakashima and H. Yamamoto, *J. Am. Chem. Soc.*, 2006, **128**, 9626–9627; (b) P. García-García, F. Lay, P. García-García, C. Rabalakos and B. List, *Angew. Chem., Int. Ed.*, 2009, **48**, 4363–4366; (c) N. Momiyama, T. Konno, Y. Furiya, T. Iwamoto and M. Terada, *J. Am. Chem. Soc.*, 2011, **133**, 19294–19297; (d) N. Momiyama, K. Funayama, H. Noda, M. Yamanaka, N. Akasaka, S. Ishida, T. Iwamoto and M. Terada, *ACS Catal.*, 2016, **6**, 949–956; (e) J. Kikuchi, H. Aramaki, H. Okamoto and M. Terada, *Chem. Sci.*, 2019, **10**, 1426–1433; (f) J. Kikuchi and M. Terada, *Angew. Chem., Int. Ed.*, 2019, **58**, 8458–8462; (g) S. A. Schwengers, C. K. De, O. Grossmann, J. A. A. Grimm, N. R. Sadlowski, G. G. Gerosa and B. List, *J. Am. Chem. Soc.*, 2021, **143**, 14835–14844.
- 15 (a) A. F. Zahrt, J. J. Henle, B. T. Rose, Y. Wang, W. T. Darrow and S. E. Denmark, *Science*, 2019, **363**, eaau5631; (b) J. P. Reid and M. S. Sigman, *Nature*, 2019, **571**, 343–348.
- 16 (a) K. Kanomata, Y. Toda, Y. Shibata, M. Yamanaka, S. Tsuzuki, I. D. Gridnev and M. Terada, *Chem. Sci.*, 2014, **5**, 3515–3523; (b) J. P. Reid and J. M. Goodman, *J. Am. Chem. Soc.*, 2016, **138**, 7910–7917; (c) P. A. Champagne and K. N. Houk, *J. Am. Chem. Soc.*, 2016, **138**, 12356–12359; (d) C. Liu, M. Besora and F. Maseras, *Chem.-Asian J.*, 2016, **11**, 411–416; (e) F. Li, T. Korenaga, T. Nakanishi, J. Kikuchi and M. Terada, *J. Am. Chem. Soc.*, 2018, **140**, 2629–2642; (f) K. Kanomata, Y. Nagasawa, M. Yamanaka, Y. Shibata, F. Egawa, J. Kikuchi and M. Terada, *Chem.-Eur. J.*, 2020, **26**, 3364–3372.
- 17 (a) A. E. Davis, J. M. Lowe and M. K. Hilinski, *Chem. Sci.*, 2021, **12**, 15947–15952; (b) S. Portela and I. Fernández, *J. Org. Chem.*, 2022, **87**, 9307–9315.
- 18 J. Chen, Y. Fu, Y. Yu, J.-R. Wang, Y.-W. Guo, H. Li and W. Wang, *Org. Lett.*, 2020, **22**, 6061–6066.
- 19 (a) J. Pous, T. Courant, G. Bernadat, B. I. Iorga, F. Blanchard and G. Masson, *J. Am. Chem. Soc.*, 2015, **137**, 11950–11953; (b) N. Momiyama, H. Tabuse, H. Noda, M. Yamanaka, T. Fujinami, K. Yamanishi, A. Izumiseki, K. Funayama, F. Egawa, S. Okada, H. Adachi and M. Terada, *J. Am. Chem. Soc.*, 2016, **138**, 11353–11359; (c) T. Varlet, C. Gelis, P. Retailleau, G. Bernadat, L. Neuville and G. Masson, *Angew. Chem., Int. Ed.*, 2020, **59**, 8491–8496.
- 20 (a) J. J. Li, *Heterocyclic Chemistry in Drug Discovery*, John Wiley & Sons, Hoboken, NJ, 2013; (b) V. Dhayalan, R. Dandela, K. V. Devi and R. Dhanusuraman, *SynOpen*, 2022, **6**, 31–57.
- 21 For M06-2X, see: Y. Zhao and D. G. Truhlar, *Theor. Chem. Acc.*, 2008, **120**, 215–241.
- 22 (a) B. R. Beno, K. N. Houk and D. A. Singleton, *J. Am. Chem. Soc.*, 1996, **118**, 9984–9985; (b) P. Vermeeren, T. A. Hamlin and F. M. Bickelhaupt, *Phys. Chem. Chem. Phys.*, 2021, **23**, 20095–20106.



- 23 For selected examples on distortion/interaction analysis in catalytic asymmetric reactions, see: (a) M. Odagi, K. Furukori, Y. Yamamoto, M. Sato, K. Iida, M. Yamanaka and K. Nagasawa, *J. Am. Chem. Soc.*, 2015, **137**, 1909–1915; (b) J. Quyang, R. Maji, M. Leutzsch, B. Mitschke and B. List, *J. Am. Chem. Soc.*, 2022, **144**, 8460–8466; (c) K. Ogura, I. Isozumi, T. Takehara, T. Suzuki and S. Nakamura, *Org. Lett.*, 2022, **24**, 8088–8092.
- 24 For natural bond orbital (NBO) analysis, see: A. E. Reed, L. A. Curtiss and F. Weinhold, *Chem. Rev.*, 1988, **88**, 899–926.
- 25 (a) S. Tsuzuki, K. Honda, T. Uchimaru, M. Mikami and A. Fujii, *J. Phys. Chem. A*, 2006, **110**, 10163–10168; (b) S. Karthikeyan, V. Ramanathan and B. K. Mishra, *J. Phys. Chem. A*, 2013, **117**, 6687–6694.
- 26 C. Hansch, A. Leo and R. W. Taft, *Chem. Rev.*, 1991, **91**, 165–195.
- 27 (a) T. Kumagai, T. Abe, Y. Fujimoto, T. Hayashi, Y. Inoue and Y. Nagao, *Heterocycles*, 1993, **36**, 1729–1734; (b) Y. Blériot, A. T. Tran, G. Prencipe, Y. Jagadeesh, N. Auberger, S. Zhu, C. Gauthier, Y. Zhang, J. Désiré, I. Adachi, A. Kato and M. Sollogoub, *Org. Lett.*, 2014, **16**, 5516–5519.
- 28 The higher the electron density of the aromatic ring, the stronger the C–H $\cdots\pi$ interaction; if the electron density of the aromatic ring is low, the strength of the C–H $\cdots\pi$ interaction is not markedly affected by the electron density of the aromatic ring. Therefore, the introduction of the electron-donating methoxy substituent leads to the enhancement of the C–H $\cdots\pi$ interaction. In contrast, the strength of the C–H $\cdots\pi$ interaction does not change markedly when an electron-withdrawing substituent is introduced to the aromatic ring, irrespective of the electron density of the aromatic ring. See: ref. 25b.
- 29 C. Eschmann, L. Song and P. R. Schreiner, *Angew. Chem., Int. Ed.*, 2021, **60**, 4823–4832.

